


THE VELOCITY COHERENCE SCALE: A NOVEL PROBE OF COSMIC HOMOGENEITY AND A POTENTIAL STANDARD RULER

LEONARDO GIANI 


Swinburne University of Technology, Hawthorn VIC 3122, Australia
School of Mathematics and Physics, The University of Queensland, Brisbane, QLD 4072, Australia and
OzGrav: The ARC Centre of Excellence for Gravitational Wave Discovery

CULLAN HOWLETT 

School of Mathematics and Physics, The University of Queensland, Brisbane, QLD 4072, Australia and
OzGrav: The ARC Centre of Excellence for Gravitational Wave Discovery

CHRIS BLAKE 

Swinburne University of Technology, Hawthorn VIC 3122, Australia and
OzGrav: The ARC Centre of Excellence for Gravitational Wave Discovery

RYAN TURNER 

The Australian National University, Canberra ACT 2601, Australia and
OzGrav: The ARC Centre of Excellence for Gravitational Wave Discovery

TAMARA M. DAVIS 

School of Mathematics and Physics, The University of Queensland, Brisbane, QLD 4072, Australia and
OzGrav: The ARC Centre of Excellence for Gravitational Wave Discovery

Version April 9, 2026

Abstract

We introduce the *velocity coherence scale* R_v , the scale at which the spherical volume average of the trace of the velocity correlation tensor transitions from scaling faster than the sphere radius to scaling more slowly. This corresponds to the radius at which the average motion of galaxies along their separation vectors transitions from correlated to anti-correlated. More intuitively, R_v represents the scale at which galaxies, on average, cease to move coherently. We derive a theoretical estimator for R_v by defining the *bulk in spheres* \mathcal{B}_R , a velocity-field analogue of the mean scale counts used in density-field correlation analyses. We show that, for a statistically homogeneous matter distribution, the logarithmic derivative of \mathcal{B}_R and the correlation dimension D_2 share the same asymptotic behaviour and therefore can be used to estimate the scale of transition to statistical homogeneity. Furthermore, we show that in standard Λ CDM cosmologies the velocity coherence scale is tightly connected to the matter–radiation equality scale k_{eq} , and that its value in comoving coordinates is redshift-independent. These results highlight the potential of R_v both as a standard ruler and as a physically motivated scale characterising the onset of cosmic homogeneity.

We present a proof of concept using measurements of the peculiar velocity correlation functions from the Sloan Digital Sky Survey. We show that the main challenge in determining R_v is the limited precision of peculiar velocity measurements compared to density ones, as they typically rely on smaller samples with larger uncertainties that scale roughly linearly with survey depth. Fitting our theoretical estimators for R_v with both a parabolic model and a third-order polynomial, we obtain $R_v \approx 132^{+29}_{-51}$ Mpc/ h . Finally, we show that more precise determinations should be achievable with current and upcoming peculiar velocity surveys.

1. INTRODUCTION

The cosmological principle posits that the Universe, on sufficiently large scales, is statistically homogeneous and isotropic. Observations broadly support this foundational assumption of the standard cosmological model, yet determining the scales at which deviations from homogeneity may bias cosmological inference remains a subtle and nuanced task.

A number of consistency tests of cosmic homogeneity have been conducted using the three-dimensional distribution of galaxies. One such test is based on the consideration that, in a homogeneous distribution, the number of galaxies contained within a sphere of radius r scales proportionally with the sphere's volume. The radius R_H at which this proportionality is reached (within a specified tolerance) provides an empirical characterisation of the transition to homogeneity (Martinez and Coles 1994; Martinez *et al.* 1998; Amendola and Palladino 1999; Pan and Coles 2000; Yadav *et al.* 2005; Sarkar *et al.* 2009; Sylos Labini *et al.* 2009a,b; Labini and Baryshev 2010; Labini 2011; Ntelis *et al.* 2017). Different estimators have been considered in the literature (Borgani 1995; Martinez and Saar 2002; Shao *et al.* 2025; Bizarria *et al.* 2025), and it has been shown that the homogeneity scale itself, if measured at different redshifts, can be used as a standard ruler within a given cosmological model (Ntelis *et al.* 2018; Avila *et al.* 2021). However, these analyses have also revealed that the transition scale measured from galaxy samples is degenerate with the galaxy bias b , which describes the proportionality between the tracer and the underlying dark matter density field. Consequently, inferring R_H for the matter distribution from galaxy surveys requires assumptions about both the cosmological model and the galaxy bias (Scrimgeour *et al.* 2012).

In this work we advocate a new method to bluecharacterise the transition-to-homogeneity scale using peculiar velocity (PV) measurements. At scales where linear cosmological perturbation theory applies, PVs offer two key advantages: they provide an unbiased (b -independent) tracer of the underlying matter distribution, and they are particularly sensitive to the largest-scale modes. Moreover, recent evidence for anomalously large bulk flows in the local Universe (Aluri *et al.* 2023; Watkins *et al.* 2023; Whitford *et al.* 2023; Watkins and Feldman 2025) provides additional motivation to investigate the transition to homogeneity using PVs as a complementary probe. This is particularly timely in view of upcoming surveys such as the Dark Energy Spectroscopic Instrument (DESI) PV survey and the 4MOST Hemispheric Surveys (4HS), as well as the growing interest in whether backreaction effects from inhomogeneities may help alleviate several current cosmological tensions (Clifton and Hyatt 2024; Giani *et al.* 2024, 2025a,b; Lane *et al.* 2025; Camarena *et al.* 2025; Galoppo *et al.* 2025).

The core idea of our approach is that inhomogeneities in the density field induce characteristic correlations in the peculiar motions of distant tracers. For example, the gravitational field of a central mass generates anti-correlated motions between galaxy pairs positioned on opposite sides of it, and correlated motions for pairs within the same hemisphere. To analyse the statistical properties of these correlations in a homogeneous matter distribution, we define the *bulk in spheres*, i.e. the spherical average of the trace of the velocity correlation tensor. We then define the *velocity coherence scale* R_v as the scale at which these averaged correlations transition from decreasing more slowly than the sphere radius to decreasing more rapidly than it. Physically, this corresponds to the scale at which, on average, the motion of galaxies within the sphere transitions from positive to negative correlation along their separation vectors. To illustrate the potential of this approach, we apply it to measurements of the PV correlation function from Ref. Lyall *et al.* (2024) for the Sloan Digital Sky Survey (SDSS) PV catalogue (Howlett *et al.* 2022), and assess the detectability of the velocity coherence scale with current and upcoming datasets.

The structure of the paper is as follows. In Section 2 we introduce peculiar velocity correlation functions, review the correlation dimension as a probe of the homogeneity scale, and introduce the velocity coherence scale and its connection with a homogeneous distribution. In Section 3 we provide a proof of concept by applying the methodology to measurements of the velocity correlation function from SDSS. Finally, Section 4 presents a discussion of our results and our conclusions.

2. THEORY

2.1. Velocity correlation functions

If the velocity field is linear, homogeneous, isotropic and irrotational, the correlation between the velocity components (i, j) of two tracers at positions A and B can be written (Gorski 1988; Groth *et al.* 1989; Wang *et al.* 2018, 2021; Turner *et al.* 2022; Blake and Turner 2023; Turner 2024)

$$\langle v_i(\vec{r}^A), v_j(\vec{r}^B) \rangle = \Psi_{ij}(r), \quad (1)$$

where we have introduced the velocity tensor

$$\Psi_{ij} = [\Psi_{\parallel}(r) - \Psi_{\perp}(r)] \hat{r}_i^A \hat{r}_j^B + \Psi_{\perp}(r) \delta_{ij}, \quad (2)$$

where r is the distance between A and B , \vec{r}^A and \vec{r}^B their positions, and the $\Psi_{\parallel, \perp}$'s describe the correlation between components of the velocity parallel and perpendicular to their separation vector respectively. In linear perturbation theory, these depend only on the variance of the density field and the growth rate of structure, with the functional dependence in Fourier space reading simply:

$$\Psi_{\parallel}(r) = \frac{H^2 a^2 f^2}{2\pi^2} \int_0^{\infty} dk P(k) \left[j_0(kr) - 2 \frac{j_1(kr)}{kr} \right], \quad \Psi_{\perp}(r) = \frac{H^2 a^2 f^2}{2\pi^2} \int_0^{\infty} dk P(k) \frac{j_1(kr)}{kr}. \quad (3)$$

Since in practice one can only measure the projection of the velocity field along the line of sight u , it is useful to define the following functions

$$\langle \Psi_1(r) \rangle = \frac{\sum_{A,B}^{r_{\text{bin}}} u_A u_B \cos \theta_{AB}}{\sum_{A,B}^{r_{\text{bin}}} \cos^2 \theta_{AB}} \quad \langle \Psi_2(r) \rangle = \frac{\sum_{A,B}^{r_{\text{bin}}} u_A u_B \cos \theta_A \cos \theta_B}{\sum_{A,B}^{r_{\text{bin}}} \cos \theta_{AB} \cos \theta_A \cos \theta_B}, \quad (4)$$

with the sums taken over all the unique ($A < B$) pairs of galaxies in the r separation bin, and where the θ 's are the angles between the position and separation vectors of the galaxies ($\cos \theta_i = \hat{r} \cdot \hat{r}_i$, $\cos \theta_{AB} = \hat{r}_A \cdot \hat{r}_B$). Ref. [Gorski \(1988\)](#) derives the following transformations between $\Psi_{1,2}$ and $\Psi_{\parallel,\perp}$

$$\langle \Psi_1(r) \rangle = \mathcal{A}(r) \Psi_{\parallel}(r) + [1 - \mathcal{A}(r)] \Psi_{\perp}(r), \quad \langle \Psi_2(r) \rangle = \mathcal{B}(r) \Psi_{\parallel}(r) + [1 - \mathcal{A}(r)] \Psi_{\perp}(r). \quad (5)$$

The functions A and B depend on the survey geometry

$$\mathcal{A} = \frac{\sum_{A,B}^{r_{\text{bin}}} w_A w_B \cos \theta_{AB}}{\sum_{A,B}^{r_{\text{bin}}} w_A w_B \cos^2 \theta_{AB}}, \quad \mathcal{B} = \frac{\sum_{A,B}^{r_{\text{bin}}} w_A w_B \cos \theta_A \cos \theta_B}{\sum_{A,B}^{r_{\text{bin}}} w_A w_B \cos \theta_{AB} \cos \theta_A \cos \theta_B}, \quad (6)$$

where the weights w account for the distance-dependent error on individual velocity measurements ($w \propto (n_g P_v + \sigma^2)^{-1}$), see for example Refs. [Qin et al. \(2019\)](#); [Turner et al. \(2021\)](#) for their detailed derivation.

2.2. Probing statistical homogeneity with the density field

Let us briefly describe how the homogeneity scale can be defined in a cosmological setting. A distribution produced by a stationary stochastic process is homogeneous and isotropic if it has a unique, position independent non-vanishing average $\langle \rho(\vec{x}) \rangle \equiv \rho_0$ and the order n moments of the distribution depend only on the relative distance between the n points. Within these assumptions, a homogeneity scale R_H can be defined from

$$\frac{1}{R^3} \int_0^R dr r^2 \xi(\vec{x}_o + \vec{r}) \rightarrow 0, \quad \forall R \geq R_H, \quad \forall \vec{x}_o \in \mathcal{V}, \quad (7)$$

where $\xi(r)$ is the usual 2-point reduced correlation function of the density contrast $\delta(\vec{x}) = (\rho(\vec{x}) - \rho_0)/\rho_0$ and \vec{x}_o the position of any galaxy within the survey volume \mathcal{V} . We address the reader to appendix [A](#) for a more formal discussion of this definition following closely Refs. ([Gabrielli and Sylos Labini 2001](#); [Gabrielli et al. 2002](#)).

In a realistic Universe containing inhomogeneities, the vanishing of Eq. (7) is reached only asymptotically. Hence, it is customary to adopt a threshold value λ to identify the transition to homogeneity with the scale R_ρ for which:

$$\left| \frac{1}{R^3} \int_0^R dr r^2 \xi(\vec{x}_o + \vec{r}) \right| \leq \lambda, \quad \forall R \geq R_\rho, \quad \forall \vec{x}_o. \quad (8)$$

An important remark is in order. It is the asymptotic behaviour of the volume average of the correlation function $\xi(r)$ that establishes whether the underlying density distribution is statistically homogeneous, whilst the choice of the threshold λ is somewhat arbitrary. In the standard cosmological model, with a standard primordial Harrison Zeldovich spectrum of perturbations $P(k) \propto k^n$ (with $n \approx 1$), we have on large scales $\xi(r) \propto r^{-(n+3)}$.

THE MEAN SCALED COUNTS AND THE CORRELATION DIMENSION

Having defined a suitable definition of homogeneity, let us move on to the description of the most common estimators usually adopted in homogeneity scale measurements: the mean scale counts \mathcal{N} and the correlation dimension D_2 . A good estimate of the mean number of neighboring tracers in a sphere of radius R centered on any galaxy is ([Peebles 1980](#)):

$$\bar{N}(R) = 4\pi\bar{\rho} \int_0^R d\bar{r} [1 + \xi(\bar{r})] \bar{r}^2, \quad (9)$$

where $\bar{\rho}$ is the mean density of the tracers and $\bar{\xi}(r)$ their real space two point correlation function. The mean scaled counts is then given by its volume average

$$\bar{\mathcal{N}}(R) = \frac{3}{4\pi R^3} \bar{N}(R), \quad (10)$$

and whose scaling with the radius essentially defines the correlation dimension D_2

$$\bar{D}_2(R) = 3 + \frac{d \ln \bar{\mathcal{N}}(R)}{d \ln R}. \quad (11)$$

Ref. [Scrimgeour et al. \(2012\)](#) advocated for the use of the following operational estimator for \mathcal{N} in a given galaxy survey

$$\mathcal{N} = \frac{1}{G} \sum_{i=1}^G \frac{N^i(< r)}{\frac{1}{R} \sum_{j=1}^{n_{\text{rand}}} w_j N_{\text{rand}^i, j}(< r)}, \quad (12)$$

where G is the number of observed tracers, and where the averaged number of objects within a random sphere N_i centered in any of them is normalized by the weighted (with weights $w_j \equiv \rho/\rho_{j, \text{rand}}$) averaged number count across n_{rand} random catalogs. These randoms are generated from a homogeneous distribution sharing the same window functions and number densities of the galaxy survey considered, which as noticed in ([Labini and Antal 2026](#)) might bias the estimator towards homogeneity.

In virtue of Eq. (7), for a homogeneous distribution we have $N(R) \propto R^3$, implying $\mathcal{N}(R) \rightarrow 1$ and $D_2 \rightarrow 3$. Since these values are reached only asymptotically, it is customary (and somewhat arbitrary) to define the homogeneity scale as the one where the correlation dimension and the mean scaled count cross the thresholds $\mathcal{N} = 1.01$ and $D_2(R_H) = 2.97$, corresponding to 1% deviation from a Poisson distribution.

Another important remark is in order: both definitions of \mathcal{N} and $\bar{\mathcal{N}}$ (and their logarithmic derivatives) rely on some degree of homogeneity. Indeed, both the definition of a correlation function $\xi(r)$ in Eq. (9) and the direction independent averaging across all the spheres in Eq. (12) presuppose translational invariance and the existence of a well defined mean density.¹ Therefore, whilst the asymptotic behaviour of these estimators can be used to define the scale of transition to homogeneity scale (within a certain threshold), they cannot be used by themselves to test the cosmological principle. An exception to this is the case of fractal Universes, for which the correlation dimension D_2 asymptotes to a different constant which depends on the value of the fractal dimension d .

2.3. The “bulk in spheres”

Let us now define an analogy of the “count in spheres” for the velocity field. A sensible choice is to compute the average on a sphere of radius R of what [Gorski \(1988\)](#) refers to as “total velocity”

$$\mathcal{B}_R = \frac{3}{R^3} \int_0^R dr (\Psi_{\parallel}(r) + 2\Psi_{\perp}(r)) r^2, \quad (13)$$

which is particularly interesting because of its connection with bulk flow measurements. Indeed, assuming Gaussian density fluctuations, the velocity field is a gaussian random variate with zero mean and variance that can be calculated from the velocity power spectrum P_{vv} ([Li et al. 2012](#); [Andersen et al. 2016](#)). Smoothing the latter over a sphere of radius R with a uniform window function $W(r)$

$$W(r) = \begin{cases} \frac{3}{4\pi R^3} & \text{if } r < R \\ 0 & \text{if } r > R \end{cases}, \quad (14)$$

one obtains²

$$\sigma_v^2(R) = \frac{H^2 f^2 a^2}{2\pi^2} \int_0^{\infty} dk P(k) \tilde{W}(k, R)^2, \quad (15)$$

where we have introduced the Fourier transform of the window function

$$\tilde{W}(k, R) = 4\pi \int_0^{\infty} dr r^2 W(r) j_0(kr) = \frac{3}{R^3} \int_0^R dr r^2 j_0(kr), \quad (16)$$

which can be used to compute the most likely value for the amplitude of the bulk flow ([Andersen et al. 2016](#))

$$|\mathbf{V}| = \frac{2}{3} \sigma_v(R). \quad (17)$$

We are now in the position of highlighting the relation between \mathcal{B}_R and the bulk flow amplitude $|\mathbf{V}|$. Substituting Eqs. (3) in Eq. (13) we can write

$$\mathcal{B}_R = \frac{3}{R^3} \frac{H^2 f^2 a^2}{2\pi^2} \int_0^{\infty} dk \int_0^R dr r^2 j_0(kr) P(k) = \frac{f^2 H^2 a^2}{2\pi^2} \int_0^{\infty} dk P(k) \tilde{W}(k, R), \quad (18)$$

which compared with Eq. (15) shows that the main difference between the two quantities is in the exponent of the window function \tilde{W} . The reason is that the standard definition of σ_R (and $\sigma_v(R)$) quantifies the correlation between the smoothed density (velocity) field at two points $\langle \delta_R(x), \delta_R(y) \rangle$, where the smoothed density field

$$\delta_R(x) = \int_0^{\infty} dy W(x-y) \delta(y), \quad (19)$$

is given by the convolution of δ with the top hat window function. Therefore, each δ_R contributes a Fourier transform of the window function in Eq. (15). In contrast, Eq. (13) is by definition the smoothed velocity correlation function, rather than the correlation function of the smoothed velocity field.³

To move forward, let us notice that on linear scales, if the velocity field is sourced by a homogeneous gaussian random density field (generating a scalar only gravitational potential), the parallel and perpendicular components of the velocity correlation functions are not independent ([Gorski 1988](#))

$$\Psi_{\parallel}(r) = \frac{d}{dr} (r\Psi_{\perp}(r)). \quad (20)$$

¹ Notice that even if the underlying density distribution is inherently direction dependent, nothing prevents one from constructing an isotropic correlation function $\xi(r)$ from the average correlation between tracers with separation r . In this case, $\xi(r)$ corresponds to the monopole of the distribution, with higher order moments expected to be non-negligible in a truly inhomogeneous distribution.

² In close analogy with the definition of the rms of the density field $\sigma(R)$, if not for the k^2 factor in the integrand and the prefactor $(Hfa)^2$.

³ Notice that indeed a similar relation holds true between the rms of the density field σ_R and the volume average of the correlation function $R^{-3} \int_0^R dr r^2 \xi(r)$, whose integrands in Fourier space differ only of a factor \tilde{W} .

Simple integration by parts allow us to write

$$\int_0^R r^2 \Psi_{\parallel}(r) = \int_0^R r^2 \frac{d}{dr}(r \Psi_{\perp}(r)) = R^3 \Psi_{\perp}(R) - \int_0^R 2r^2 \Psi_{\perp}(r) , \quad (21)$$

and conclude, by inserting this expression into Eq. (13), that a suitable expectation is $\bar{\mathcal{B}}_R = 3\Psi_{\perp}(R)$ (a bar indicates that this is the total velocity one would obtain *if* the velocity field is irrotational and sourced by a scalar random density field, and may not be equal to what one would measure if the Universe is inhomogeneous, anisotropic or does not obey these assumptions). We can also define an analogous statistic \mathcal{S} to the correlation dimension D_2 for \mathcal{B}_R :

$$\mathcal{S}(R) = \frac{d}{dR} (R\mathcal{B}_R) , \quad (22)$$

where we included a factor of R in the parenthesis because, under the same assumptions as in Eq. (20), one can show that $\bar{\mathcal{S}} = \Psi_{\parallel}$, which facilitates its physical interpretation.

SCALING OF \mathcal{B}_R AND THE TRANSITION TO HOMOGENEITY

As mentioned above, while the specific threshold λ used to define the homogeneity scale is arbitrary, it is the asymptotic behaviour of the volume average of the correlation function (and its scaling D_2) that determines whether a distribution is homogeneous. In this section, we show that this asymptotic behaviour is captured in the same way by the scaling of both \mathcal{N} and \mathcal{B}_R . Indeed, apart from constant (or redshift-dependent) multiplicative amplitude factors, the radial dependence of \mathcal{N} and \mathcal{B}_R can be written as

$$\mathcal{N}(R) \propto I_1(R) = \int dk k^2 P(k) \tilde{W}(k, R) , \quad (23)$$

$$\mathcal{B}_R(R) \propto I_2(R) = \int dk P(k) \tilde{W}(k, R) . \quad (24)$$

For a fiducial Λ CDM power spectrum $P(k)$ computed using CLASS (Lesgourgues 2011), the ratio of the logarithmic derivatives of I_1 and I_2 is shown in Fig. 1. Remarkably, beyond the BAO peak, this ratio as a function of R approaches

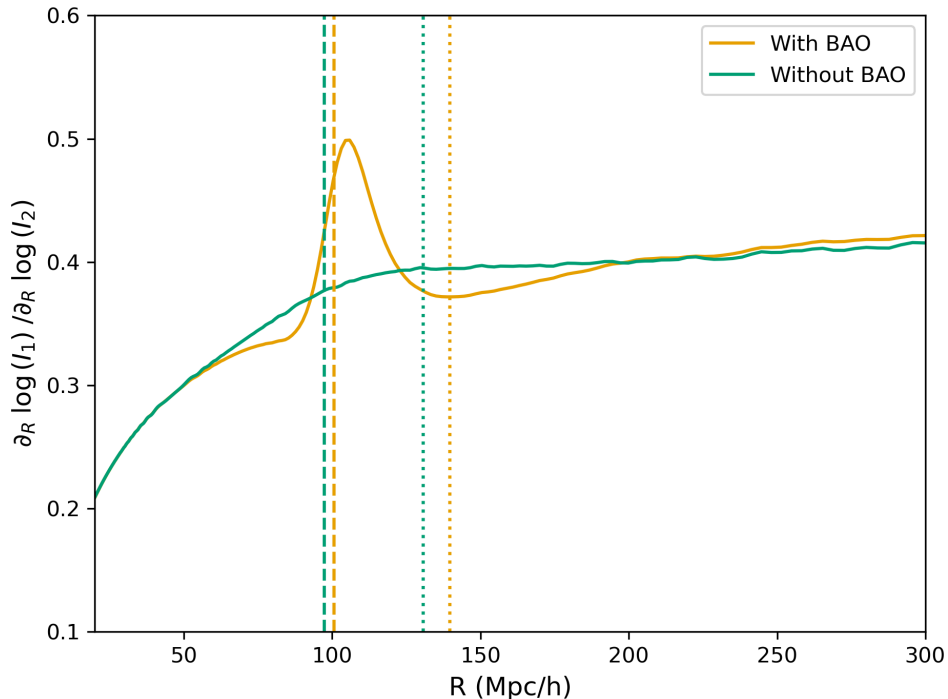


FIG. 1.— The ratio of the logarithmic derivatives of the integrals in Eqs. (23) and (24), capturing the asymptotic behaviour of the proportional scalings of \mathcal{N} and \mathcal{B}_R . The green solid curve is obtained by removing the BAO feature through Gaussian smoothing of the $P(k)$ wiggles. The dashed vertical lines correspond to the velocity coherence scales defined by Eq. (25), whereas the dotted vertical lines correspond to the density homogeneity scale R_ρ . In both cases, at sufficiently large scales the ratio approaches a constant value, highlighting the shared asymptotic scaling of the estimators \mathcal{N} and \mathcal{B}_R .

a constant value, indicating that on sufficiently large scales \mathcal{B}_R and \mathcal{N} share the same asymptotic behaviour. In the

figure, the dashed blue lines correspond to the scale R at which the product $R\mathcal{B}_R$ reaches its maximum. We argue that this provides an excellent proxy for identifying the scale at which the ratio becomes approximately constant when the BAO peak is removed (green line). Interestingly, the numerical value of R_v does not change significantly even in the presence of the BAO feature (orange line).

2.4. The velocity coherence scale

The evolution of \mathcal{B}_R as a function of radius exhibits a very interesting feature. As one might naively expect from its close correspondence with the bulk flow amplitude, it is a decreasing function of the sphere radius. However, on small scales, larger fluctuations of the density field induce strongly correlated motions, causing \mathcal{B}_R to decrease at a slower rate than on large scales. In particular, as shown in Fig. 2, \mathcal{B}_R decreases more slowly than R^{-1} below a certain scale, corresponding to a maximum in $R\mathcal{B}_R$, and faster beyond it. This maximum corresponds to a zero of \mathcal{S} , the derivative of $R\mathcal{B}_R$, and it is what we define as the *velocity coherence scale* R_v , satisfying

$$\mathcal{S}(R_v) = 0, \quad \sup(R\mathcal{B}_R)_{\forall R} = R_v\mathcal{B}_R(R_v). \quad (25)$$

As shown in Fig. 1, the velocity coherence scale can be used as a pivot scale to identify the sphere size at which \mathcal{N} and \mathcal{B}_R transition to the same asymptotic scaling. Since it is precisely the asymptotic scaling of the volume-averaged correlation function that defines the homogeneity of a matter distribution, we advocate that R_v , just like R_ρ , can be used to estimate the transition to cosmic homogeneity.

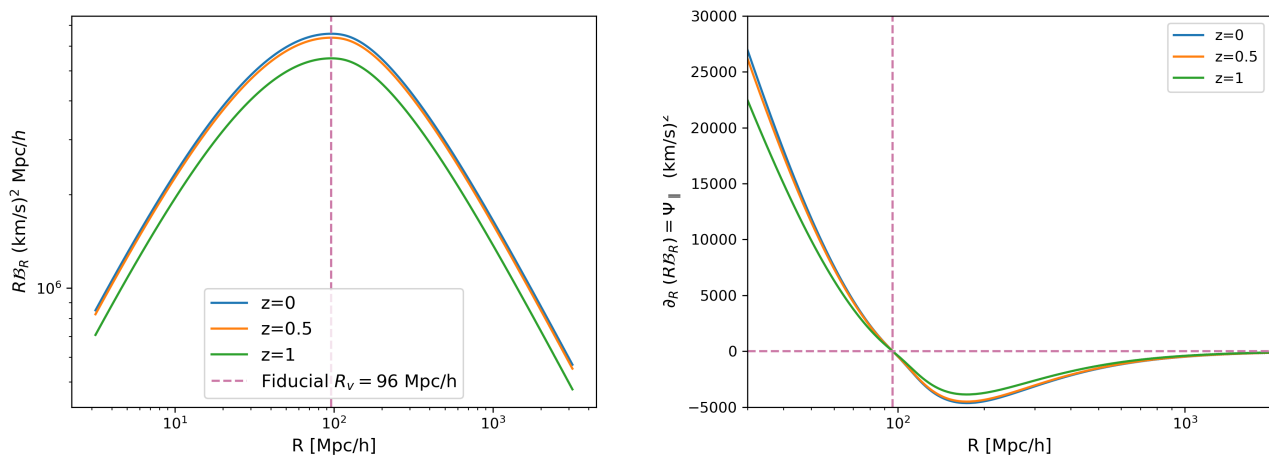


FIG. 2.— The function $R\mathcal{B}_R$ and its derivative for a fiducial Λ CDM cosmology. We identify the homogeneity scale with the transition from correlated to anticorrelated averaged velocities along the vector separation of galaxy pairs ($\Psi_{\parallel} = 0$), corresponding to a change in slope in the radial evolution of \mathcal{B}_R and the smoothed velocity variance σ_v .

Notice that since in linear theory $\mathcal{S} = \Psi_{\parallel}$, the identification of the first zero of \mathcal{S} with the scale of transition to homogeneity has a straightforward physical interpretation: the zero crossing of Ψ_{\parallel} signals that no external potential gradient is sourcing coherent flows throughout the sphere (see Fig. 3 for a diagrammatic representation).

We are now left with two statistics, \mathcal{B}_R and \mathcal{S} , and a theoretical prediction relating them in a homogeneous and isotropic universe to Ψ_{\parallel} and Ψ_{\perp} , which are themselves connected by Eq. (20).

R_V SENSITIVITY TO LONG-RANGE CORRELATIONS

A key feature of the peculiar velocity (PV) field is that it is much more sensitive to large-scale density modes than to small-scale ones, reflecting the k^{-1} suppression arising from the Euler equation. For this reason, we expect \mathcal{B}_R and \mathcal{S} to be much more sensitive to large-scale correlations than \mathcal{N} and D_2 . To illustrate that this is indeed the case, we consider a set of toy models for the power spectrum $P(k)$ in which the Harrison–Zeldovich behaviour at $k \leq k_{eq}$ is replaced with power laws $P(k) \propto k^n$ with $n \neq n_s$. We also include a toy model with $n = -1$, which is still homogeneous according to the definition given in Appendix A, but for which $\int \xi(r) \rightarrow \infty$ as $r \rightarrow \infty$. This behaviour, as argued in Ref. Gabrielli *et al.* (2002), is typical of thermodynamical systems at the critical point of a second-order phase transition, which exhibit large-scale critical correlations.

We plot the $P(k)$ and the corresponding correlation functions $\xi(r)$ in Fig. 4, explicitly showing the emergence of large-scale correlations in the $n = -1$ case (blue line).

In Fig. 5 we compare the correlation dimension D_2 and \mathcal{S} computed for these toy models, together with the corresponding thresholds for R_ρ and R_v . Whilst all the distributions have well-behaved asymptotic values of $D_2 \rightarrow 3$, we notice that for the case $n = -1$ a velocity coherence scale is not defined, since \mathcal{S} never vanishes.⁴ We conclude

⁴ In hindsight, this is easily explained by the lack of a k^2 scaling in the integral of $P(k)$ entering the velocity correlation functions.

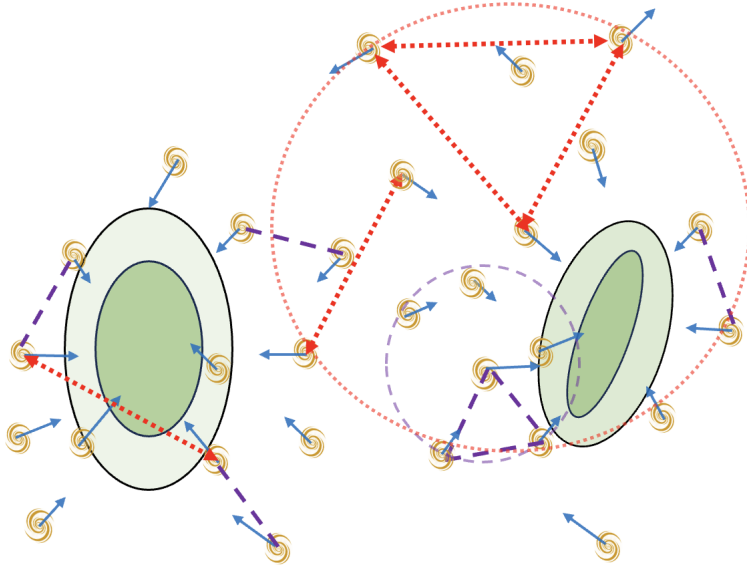


FIG. 3.— Acting on small scales (purple dashed lines), density gradients on large scales source collective flows towards a common attractor (green ellipses), resulting in a positive correlation ($\Psi_{\parallel} > 0$). The lack of strong density perturbations on large scales, on the other hand, causes galaxies to move in opposite directions rather than together (red dotted lines), contributing a negative Ψ_{\parallel} . The homogeneity scale corresponds to the scale at which $\Psi_{\parallel} = 0$, i.e. where galaxy motions with respect to each other are, on average, uncorrelated.

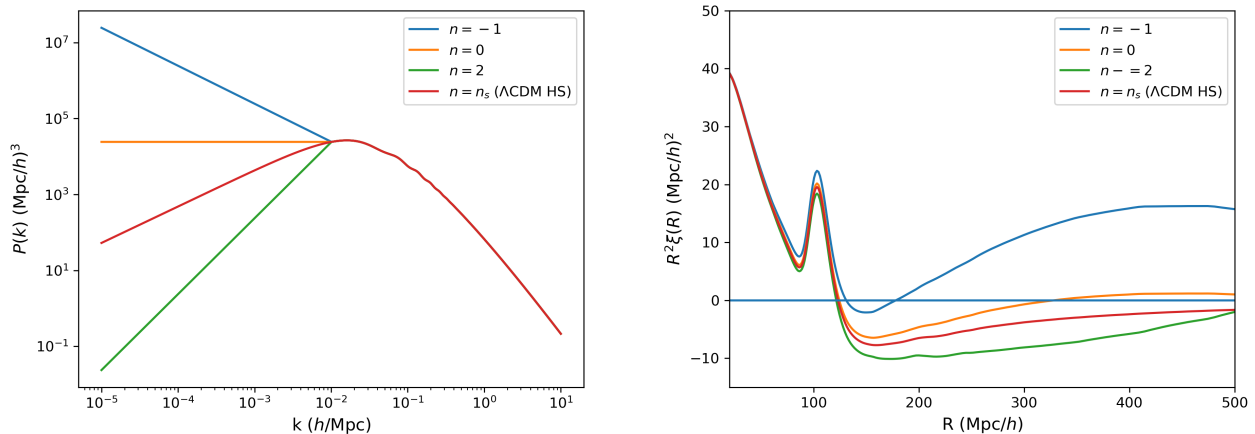


FIG. 4.— The toy models of $P(k)$ and their corresponding correlation functions $\xi(r)$ used to compare distributions with different homogeneity properties.

that whilst the existence of a velocity coherence scale ensures the existence of a homogeneity scale, the opposite is not necessarily true. In particular, for R_v to exist one cannot have long-range fluctuations (i.e. super-Poissonian), and at large scales we must have $P(k) \propto k^n$ with $n \geq 0$, corresponding to at least Poissonian noise or sub-Poissonian (superhomogeneous) fluctuations according to the terminology of Ref. [Gabrielli *et al.* \(2002\)](#).

This simple exercise highlights the differences between R_v and R_ρ , showing that the former, beyond providing complementary information on the transition to homogeneity, is particularly sensitive to large-scale correlations in the density field that are forbidden in the standard cosmological model and its Harrison–Zeldovich power spectrum of primordial perturbations. Furthermore, as we show explicitly in Appendix B by directly comparing the values of R_v and R_ρ computed across different cosmologies, the 1% threshold used to define R_ρ makes its numerical value quite susceptible to the BAO scale and amplitude. This occurs because minimal changes in the cosmological parameters can shift the flattening of the D_2 curve after the BAO peak just above or below the 2.97 threshold, leading in extreme cases to $\approx 20\%$ variations in R_ρ induced by less than a 1.5% variation in H_0 , (despite the identical asymptotic behaviour of the correlation functions). In turn, this makes the comparison of the homogeneity scale across different datasets prone to biases if, for example, their fiducial H_0 values are not in perfect agreement. In contrast, as we will show later, the velocity coherence scale R_v is mostly sensitive to k_{eq} and varies continuously with it.

2.5. R_v and its potential use as a standard ruler

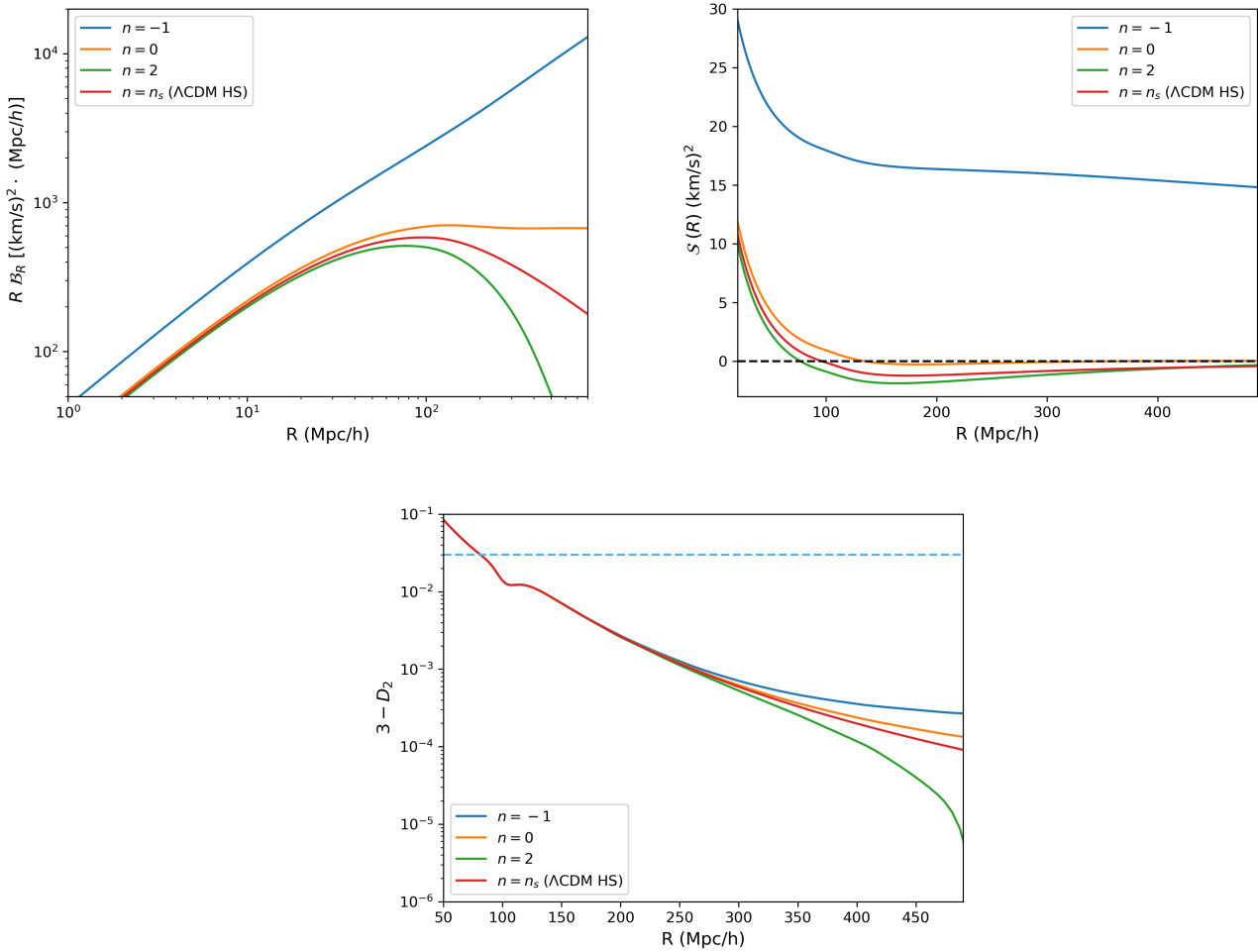


FIG. 5.— *Upper panels*: evolution of $R\mathcal{B}_R$ and S as a function of distance for the toy models of $P(k)$ shown in Fig. 4. The lack of a well-defined maximum in the top-left panel and of a zero-crossing in the top-right panel for the case $n = -1$ highlights that R_v only exists when the volume integral of the correlation function does not diverge as $R \rightarrow \infty$. *Bottom panel*: the homogeneity scale R_ρ , identified with the intersection of the curves with the threshold $D_2 = 2.97$, is essentially the same for all the models considered. Nevertheless, differences in the asymptotic behaviour of the curves grow with the radius R .

Fig. 2 shows an interesting feature of the velocity coherence scale: its value in comoving coordinates (Mpc/h) is redshift independent. This is easily explained by the fact that in linear theory the time evolution of the velocity correlation functions is entirely encoded in the amplitude factors multiplying the integrals in Eqs. (3). Therefore, whilst the overall amplitude of the correlation functions evolves with time, the location of the maximum in $R\mathcal{B}_R$ remains constant. In Appendix C we show, using “triangular” toy models of $P(k)$, that the value of R_v is essentially determined by the value of k_{eq} , or equivalently by ω_m and the baryon fraction. Therefore, the velocity coherence scale can serve as a standard ruler in the same way as the turnover scale of the matter power spectrum (Poole *et al.* 2013). That the velocity field carries information about this scale has been noted, for example, in Ref. Lai *et al.* (2025).

Inspired by the form of the analytical solutions obtained for the toy models in Eqs. (C4), we postulate the following analytical relation between R_v and k_{eq} :

$$R_v(k_{eq}) \approx \frac{\alpha}{k_{eq}} + \beta k_{eq} + \gamma. \quad (26)$$

We fit this expression numerically to the values of R_v computed using CLASS, varying ω_m in the range $0.01 \leq \omega_m \leq 0.3$ while fixing the present-day matter density to $\Omega_m = 0.31$ and the baryon fraction to $f_b = 0.156$, and keeping the remaining parameters consistent with the Planck 2018 best-fit cosmology (Aghanim *et al.* 2020). We obtain the best-fit coefficients

$$\alpha \approx 0.108, \quad \beta \approx -1960, \quad \gamma \approx 101, \quad (27)$$

with the best fit and the residuals shown in Fig. 6. The figure also shows the numerical evaluation of R_v obtained from non-linear computations of $P(k)$ in CLASS using `halofit`. As shown by the similar residuals, the numerical fit

for $R_v(k_{eq})$ remains satisfactory (with maximum deviations from the CLASS output below 3 %) even in the presence of non-linear modes.

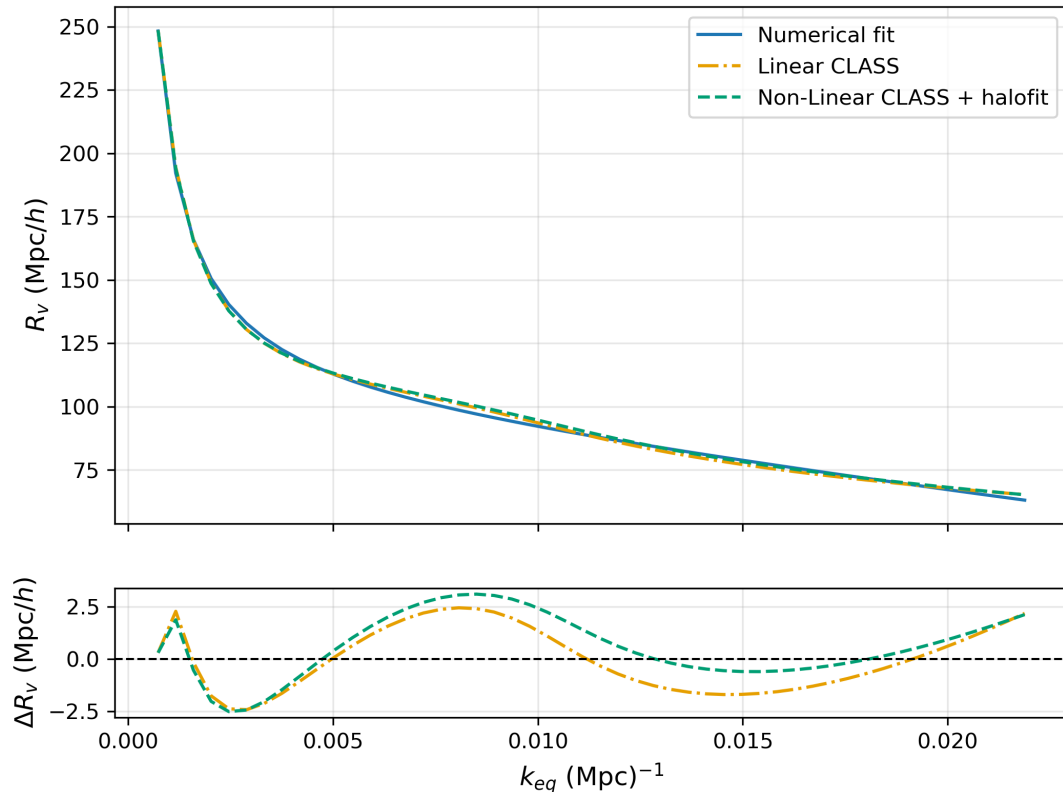


FIG. 6.— The value of R_v as a function of k_{eq} obtained while keeping fixed the present-day matter density Ω_m and the baryon fraction f_b , using both the linear (dot-dashed orange line) and non-linear (dashed green line) $P(k)$. The solid blue line shows the best-fit prediction of the parametric model in Eq. (26) to the linear $P(k)$. The bottom panel shows that the residuals in both cases are small and remain below 2% across the entire k_{eq} range.

3. PROOF OF CONCEPT ON SDSS DATA

To assess whether measurements of R_v are within the reach of current cosmological surveys, we attempt to infer it from measurements of the velocity correlation functions obtained in Lyall *et al.* (2024) from the Sloan Digital Sky Survey (SDSS) and its companion suite of 2048 mocks (Howlett *et al.* 2022), which is the largest homogeneously-selected publicly-available PV catalogue. The data consists of $\approx 34,000$ measurements of distances of early type elliptical galaxies obtained using the fundamental plane empirical relation, with a mean distance error across the dataset of $\approx 23\%$. After subtracting the homogeneous Hubble flow, these distances are converted in measurements of PVs over a sky area of 7000 deg^2 up to a redshift $z = 0.1$. These observations were compressed into summary statistics comprising 25 equally spaced binned measurements of $\Psi_{\parallel}(r)$ and $\Psi_{\perp}(r)$ up to a distance of 150Mpc/h.

Fig. 7 shows these measurements for the data, a fiducial Λ CDM cosmology, the individual mocks and their mean.

We identified R_v with the turnover point in $R\mathcal{B}_R$, which as we shown is proportional to $R\Psi_{\perp}(R)$ using Eq. (20). Consistency also requires that the same scale corresponds to the zero crossing of $\Psi_{\parallel}(R)$. As such, we look for the peak in $R\mathcal{B}_R$ adopting the same methodology used in searches of the turnover scale of the matter power spectrum, see e.g. Blake and Bridle (2005), by fitting $R\Psi_{\perp}$ using a piece-wise parabolic function

$$R\mathcal{B}_R^{\text{model}} = 3R\bar{\Psi}_{\perp} = \begin{cases} C(1 - \alpha x^2) & \text{if } R < R_v \\ C(1 - \beta x^2) & \text{if } R \geq R_v \end{cases} \quad x = (R - R_v)/R_v. \quad (28)$$

At the same time, we look for the zero crossing of Ψ_{\parallel} by modeling it with a third order polynomial

$$\Psi_{\parallel} = c_0 + c_1 R + c_2 R^2 + c_3 R^3, \quad (29)$$

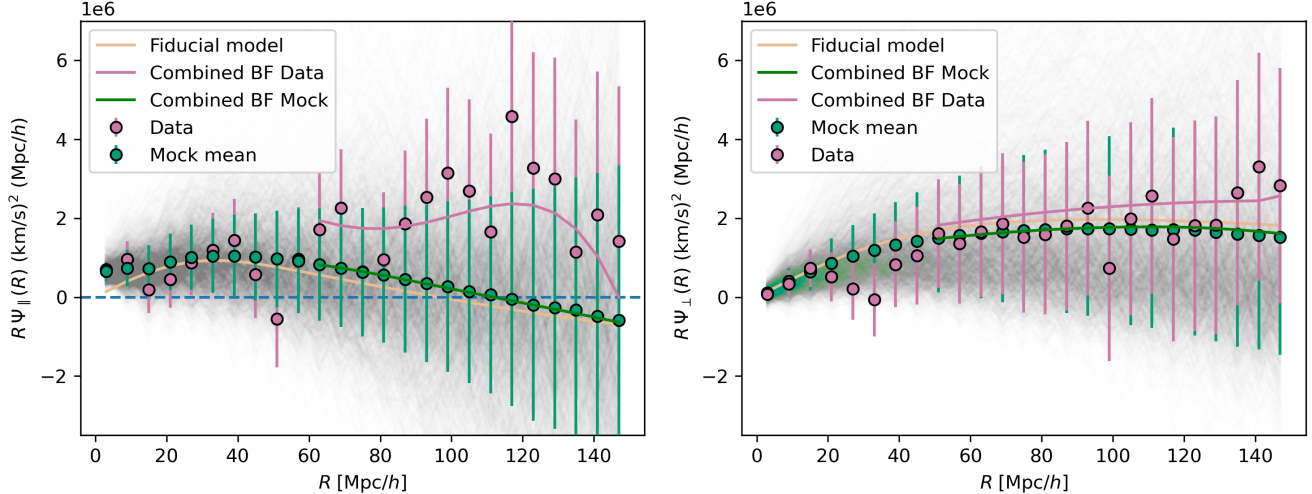


FIG. 7.— The functions Ψ_{\parallel} and Ψ_{\perp} for the SDSS data (pink), each mock realization (faint solid gray lines) together with their mean (green dots) and the fiducial cosmology used to build the mocks (orange). The solid pink and green lines correspond to the best fit results from our MCMC analysis (see Figs. 8,9 and Sec. 3). One can easily see that whilst the mean of the mocks recovers very well the input fiducial model, the distribution of the mocks around this mean is skewed and non-gaussian.

noticing that the zero crossing condition at the homogeneity scale fixes the coefficient c_0 to be

$$c_0 = -(c_1 R_v + c_2 R_v^2 + c_3 R_v^3). \quad (30)$$

The choice of a third order polynomial has no physical motivation, but introduces the same number of free parameters as in the parabolic model for $R\Psi_{\perp}$, allowing for a fairer comparison of the two estimators. We also verified that increasing the number of free parameters does not improve appreciably the fit.

We perform an MCMC exploration of the parameter space for the variables $C, \alpha, \beta, c_1, c_2, c_3$ and R_H using the *emcee* ensemble sampler, and *ChainConsumer* to analyse our chains (Foreman-Mackey *et al.* 2013; Hinton 2016).⁵ We use a Gaussian likelihood

$$\log \mathcal{L}_{\text{Gaussian}} = \sum_i -\frac{1}{2} \left[(d^i - m^i)^T \text{Cov}_{ij}^{-1} (d^j - m^j) \right], \quad (31)$$

where the subscripts i, j runs over the binned measurements, and where the data-vector d_i is constructed by stacking measurements of $R\Psi_{\perp}(R)$ and $\Psi_{\perp}(R)$, Cov_{ij} being their covariance computed from the 2048 mock realisations, and where the model predictions m_i are obtained from Eqs. (28) and (29). To avoid contamination from small-scale non-linearities in the zero-crossing and turnaround fitting, we restrict our analysis to measurements above 40 Mpc/h. Since $R\mathcal{B}_R$ is positive, following the same prescription used for $P(k)$ in Blake and Bridle (2005), we must require $\alpha, \beta \leq 1$. We adopt uniform priors $-1 \leq [\alpha, \beta] \leq 1$, $10^5 \leq C \leq 10^8$, $-50000 < c_1 < 50000$, $-100 \leq [c_2, c_3] \leq 100$ and $10 \leq R_v \leq 200$.⁶ Fig. 8 shows the results of our analysis for the mocks, fitting jointly or separately (with the appropriate subsets of the full covariance matrix) the mock mean using the turnaround and polynomial models for Ψ_{\parallel} and $R\Psi_{\perp}$. The resulting $R_v \approx 106_{-38}^{+44}$ Mpc/h is compatible with the value computed for the fiducial Λ CDM cosmology used to produce the 2048 mocks $R_v \approx 96$ Mpc/h. Fig. 9 shows instead the results of our pipeline for the SDSS data.

We found that both the mock mean and the data provide consistent marginalised constraints on the velocity coherence scale R_v , with the best fit for the combined data being $R_v \approx 132_{-51}^{+29}$ Mpc/h. The results on R_v from fitting individually Ψ_{\parallel} and Ψ_{\perp} are also consistent, with $R_v^{\Psi_{\perp}} \geq 90$ Mpc/h (68% lower bound) and $R_v^{\Psi_{\parallel}} = 60_{-44}^{+25}$ Mpc/h for the data, and $R_v^{\Psi_{\perp}} \geq 95$ Mpc/h (68% lower bound) and $R_v^{\Psi_{\parallel}} = 99_{-40}^{+49}$ Mpc/h for the mocks.

Given the quite large $\approx 25\%$ uncertainty on the measurement, one could ask whether the accuracy of this method will improve with upcoming PV datasets. To answer, we apply the same analysis to a set of measurements centered on the mock mean, but artificially decreasing their uncertainties by decreasing the covariance matrix by a factor 5. Fig. 10 shows a comparison of the results. Whilst the constraints on the polynomial-fit parameters c_i improve substantially, the uncertainties on the turnover fit and on the inferred homogeneity scale change only marginally. We argue that this is a consequence of the weak constraints on the parameter describing the parabolic downfall β . In hindsight, this is expected since SDSS measurements of the Ψ 's extend only up to 150 Mpc/h, and the best fits indicate an homogeneity scale close to this upper bound. We conclude that to improve significantly the constraints on R_v , one would also need measurements of the Ψ 's at larger scales — and that doing this even for current data may result in

⁵ Available at <https://emcee.readthedocs.io/en/stable/> and <https://samreay.github.io/ChainConsumer/>

⁶ To assess the convergence of the chains we follow the prescription given in <https://emcee.readthedocs.io/en/stable/user/autocorr/> and check the estimated autocorrelation time τ every 100 steps for each chain, considering it convergent if the estimate has changed by less than 1%.

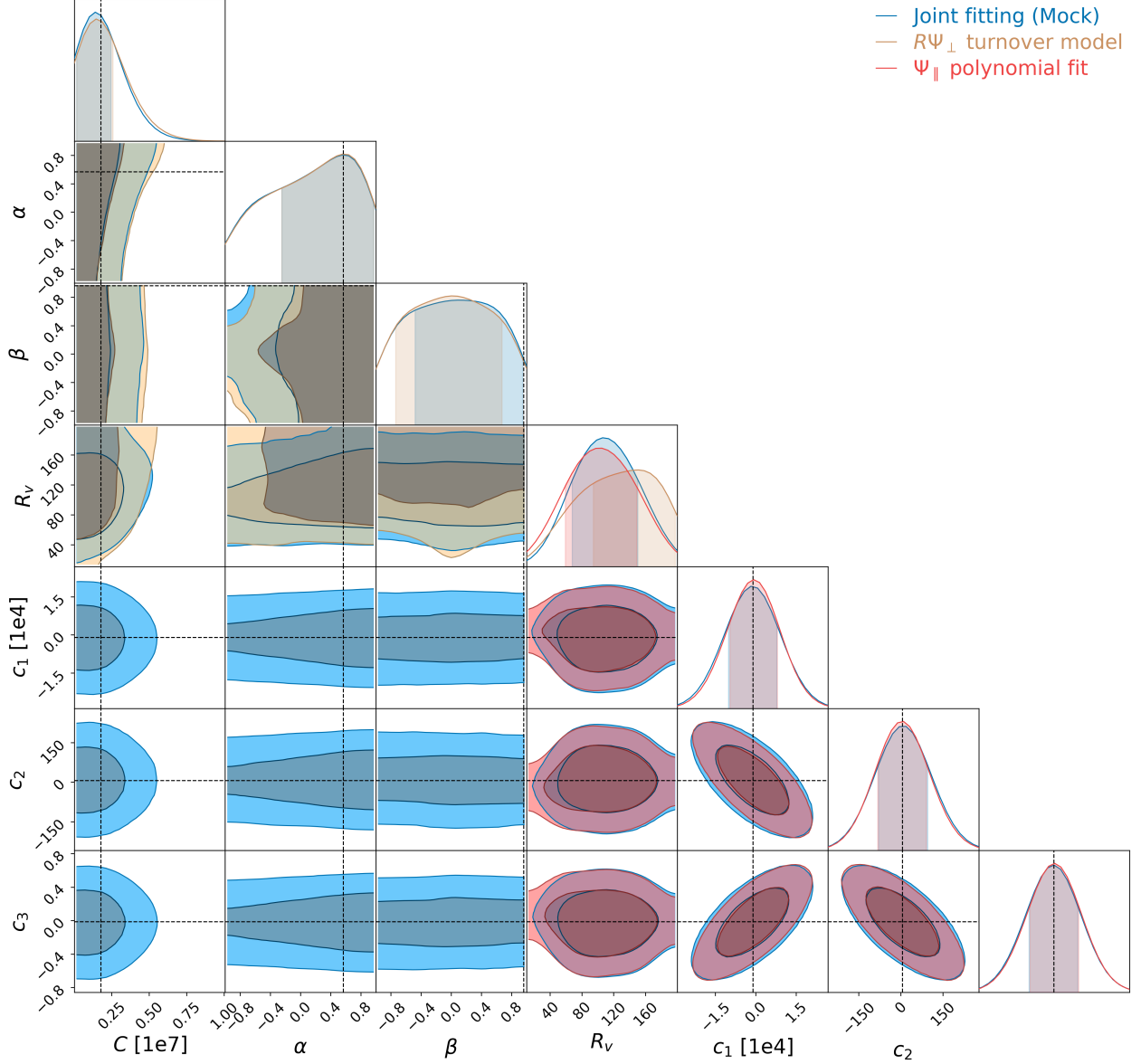


FIG. 8.— The results of our MCMC explorations for the models defined in Eqs. (28),(29) fitted to the mock mean separately (orange and red) or jointly (blue).

slightly improved constraints on R_v compared to those presented here. Are such improvements feasible? As shown for example in Blake and Turner (2023) (see appendix B therein for the detailed derivation), the covariance matrix of the velocity correlation function scales with the inverse volume. Therefore, PV surveys with the same precision and depth as the SDSS PV catalogue, but covering 5 times more sky area, are expected to at least mimic the constraining power of the blue contours in Fig. 10. Interestingly, this is roughly the improvement in sky area one would expect combining DESI (14000 deg²) Saulder *et al.* (2023); Said *et al.* (2025) and 4HS⁷ (17000 deg²) de Jong (2019). In addition to these improvements in sky coverage, these surveys will add higher number density of galaxies and richer depth (2-3 times more galaxies up to redshift $z \leq 0.15$ for DESI). This ≈ 200 Mpc/ h increase in depth will likely allow us to extend measurements of the Ψ 's to higher distances, and constrain with greater precision β .⁸

⁷ <https://4mosthemispheresurvey.github.io/>

⁸ During the preparation of this paper, the DESI collaboration released in Turner *et al.* (2025) a measurement of the Ψ 's from their first data release (DR1). As discussed in the paper, these measurements extends only up to 150 Mpc/ h due to the small sky coverage of the

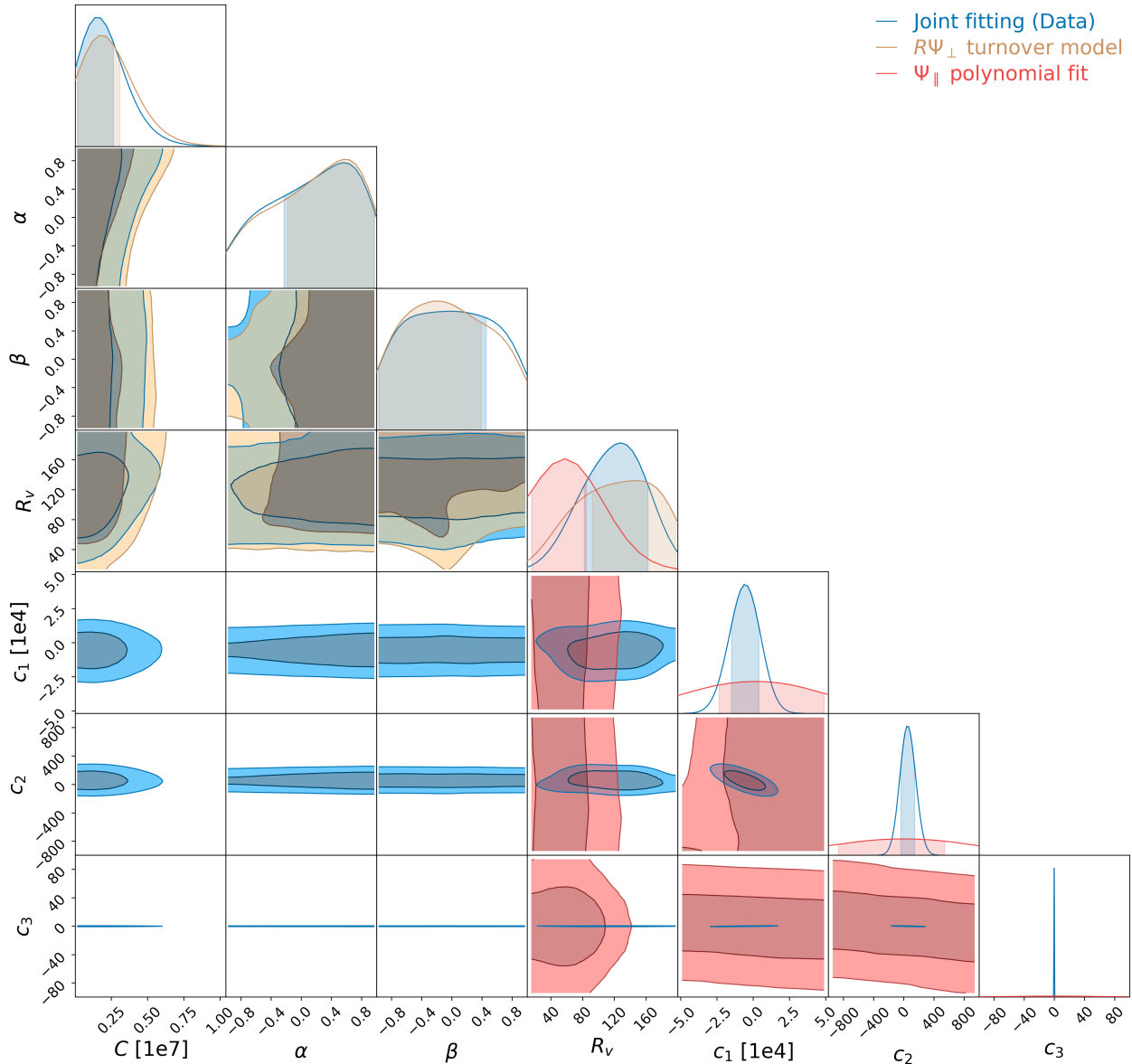


FIG. 9.— As in Fig. 8, but for the SDSS data. Compared to the results from the mocks, the parameters of the polynomial fitting of Ψ_{\parallel} are much less constrained. This is non-surprising given the noticeable difference between the green and pink lines in the left panel of Fig. 7.

We conclude that measurements of the velocity coherence scale with the methodology proposed in this paper will be feasible with greater than 20% precision in the near future. An exact estimate is, however, beyond the scope of this work, whose main objective is to provide a proof of concept of the proposed methodology. Future measurements would indeed require the production of mocks for these surveys, in order to properly account for the high correlation between the Ψ_{\parallel} and Ψ_{\perp} measurements. Moreover, the robustness of the R_v inference from Ψ 's measurements in presence of non-trivial window functions, and possible biases induced by lack of depth, different bin sizing, fitting range and alternative parametrizations to the ones in Eqs. (28),(29) should be thoroughly analyzed in order to claim a robust measurement.

4. DISCUSSION

DR1 PV sample, which will however increase significantly with the DR2 data.

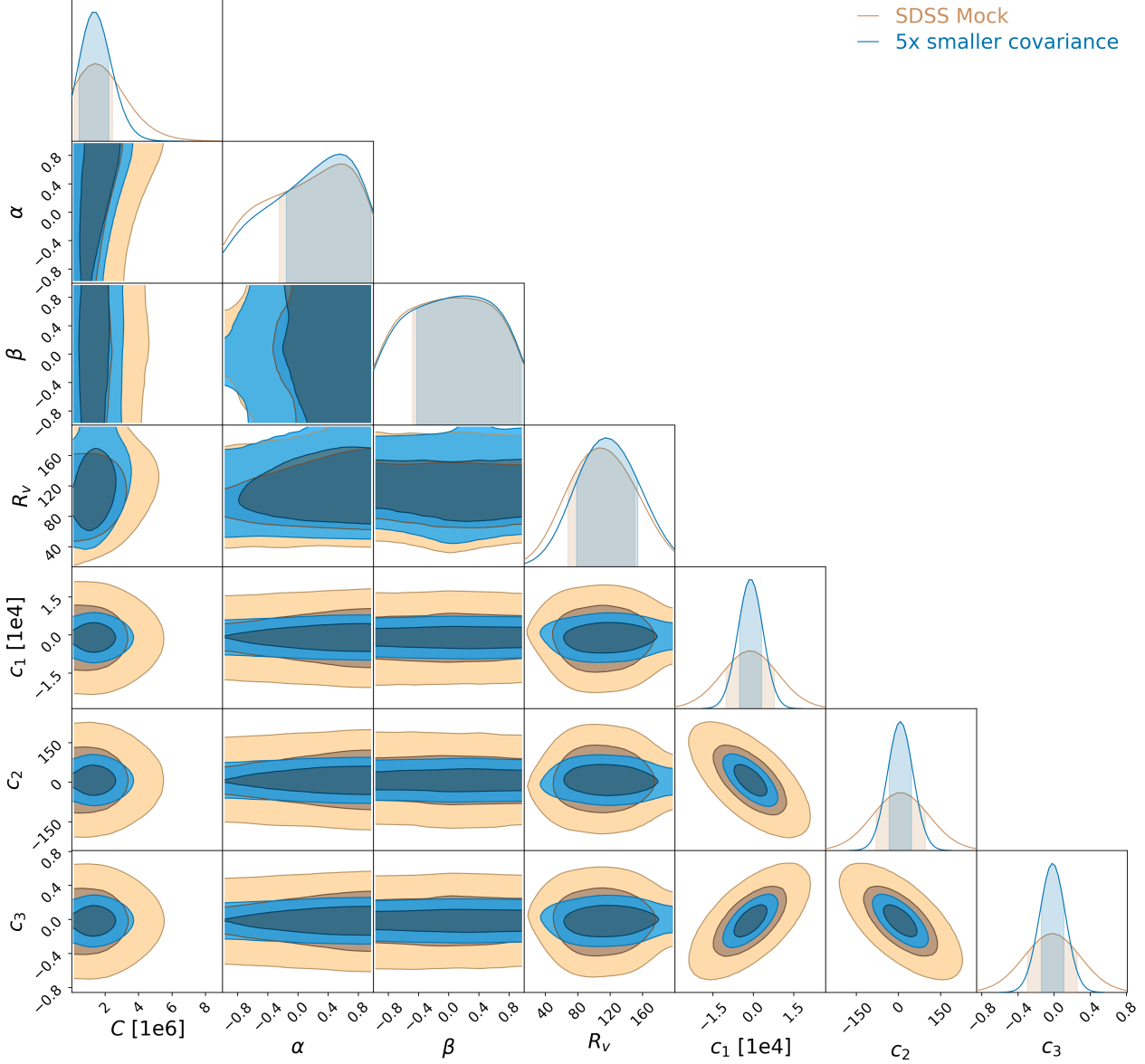


FIG. 10.— A comparison between the posteriors obtained using the covariance matrix of the mock realizations with and without an artificial factor of 5 decrease in uncertainties. We notice that the constraints on the parameters in the polynomial fit of Ψ_{\parallel} measurements increase significantly, but not much constraining power is added to the turnover fit parameters nor the velocity coherence scale R_v .

This paper advocates a new choice of threshold to define the transition to statistical homogeneity based on PV measurements. As discussed in Sec. 2.4, this can be identified with the scale R_v at which the average parallel component of the peculiar velocities of galaxy pairs transitions from correlated to anti-correlated, corresponding to the zero crossing $\Psi_{\parallel}(R_v) = 0$, and the change in slope of $R\Psi_{\perp}$. Indeed, this roughly corresponds to the scale at which the evolution of the correlation dimension D_2 and the scaling of the bulk in spheres $\partial_R \log \mathcal{B}_R$ become proportional, as shown in Fig. 1.

This definition has several key advantages. Unlike the scale R_{ρ} measured from the correlation dimension D_2 and the mean scaled counts \mathcal{N}_R , it is insensitive to (and therefore not degenerate with) the galaxy bias. Furthermore, unlike R_{ρ} , the numerical value of R_v is largely unaffected by the specific location and amplitude of the BAO peak, as demonstrated in Fig. 11.

It is well known that R_{ρ} evolves with redshift (Ntelis *et al.* 2017; Avila *et al.* 2021), as one would expect from the

non-trivial redshift dependence of σ_R and its specific numerical value. Interestingly, however, the zero crossing of $\mathcal{S}(R)$ occurs at approximately the same comoving scale at all redshifts. This can be understood by considering Eqs. (20), (22) and the theoretical estimator for Ψ_{\parallel} in Eq. (3). In the linear regime, the redshift evolution contributes only an overall rescaling of the amplitude of the power spectrum $P(k)$ (in comoving Fourier scales h/Mpc) through the growth factor $D(z)$ and the prefactors $H^2 f^2 a^2$. This overall normalization cannot significantly change the location of the peak in $R\mathcal{B}_R$, but only its amplitude, as illustrated in Fig. 2.

These considerations show that there is no simple mapping between R_v and R_ρ , as it is not possible to redefine the threshold used for D_2 so that their values match at all redshifts (which is expected, as they measure intrinsically different things). On the other hand, the proportionality between D_2 and the derivative of \mathcal{B}_R —which, unlike the thresholds R_v and R_ρ , are the actual estimators of statistical homogeneity—is redshift independent.

As discussed in Sec. 2 and Appendix B, and explicitly shown in Fig. 26, R_v is essentially determined by the value of k_{eq} . We therefore speculate that, once measured and calibrated at a given redshift, measurements of R_v could be used as a standard ruler. We caution that, in order to validate this speculation, the impact of possible systematics induced by non-linearities, selection effects, and calibration biases should be thoroughly tested using large suites of cosmological simulations.

Our analysis of SDSS data shows that existing measurements can determine R_v only with an uncertainty of approximately 20%. However, as discussed in Sec. 3, we expect that ongoing and upcoming PV surveys such as DESI, 4HS, and LSST will be able to achieve significantly higher precision in the foreseeable future.

Finally, the close analogy between Eqs. (15) and (13) points to a promising direction for future developments: reformulating the velocity coherence scale inference in terms of bulk-flow observables rather than Ψ_{\parallel} and Ψ_{\perp} . Such an approach may result in alternative estimators of the velocity correlation functions, and provide a more direct link between large-scale dynamics and the emergence of cosmic homogeneity.

We are grateful to Sunny Vagnozzi, Stefano Camera, Madeline Lily Cross-Parkin, Eric Thrane, Valerio Marra and Agne Semenaite for useful comments and suggestions. This research was conducted by the Australian Research Council Centre of Excellence for Gravitational Wave Discovery (project number CE230100016) and funded by the Australian Government.

APPENDIX HOMOGENEOUS DISTRIBUTIONS

A field ρ generated by a stationary stochastic process is homogeneous if its probability density functional $\mathcal{P}[\rho(\vec{x})]$ is translationally invariant. This is equivalent to demanding that its ensemble-average has a well-defined and position-independent value $\langle \rho(\vec{x}) \rangle \equiv \rho_0$. Furthermore, higher order n moments must depend only on the vector separations between the n points. In terms of the two point correlation function, this implies

$$C(\vec{x}, \vec{y}) = \langle \rho(\vec{x}), \rho(\vec{y}) \rangle \equiv C(\vec{x} - \vec{y}), \quad (\text{A1})$$

which, further assuming statistical isotropy, becomes a function of the scalar separation only $C \equiv C(r)$ (where $r = \sqrt{|\vec{x} - \vec{y}|^2}$). Finally, a crucial assumption for cosmological applications is that the probability density $\mathcal{P}[\rho]$ is ergodic, which usually allows one to replace the ensemble average $\langle \cdot \rangle$ with the spatial average over the total volume (infinite in the thermodynamic limit) of an individual realization of the field. This property is usually referred to as the self-averaging property of the distribution. When considering an intrinsically discrete distribution of tracers, i.e. a density distribution of the form

$$\rho(\vec{r}) = \sum_i^N \delta(\vec{r} - \vec{r}_i), \quad (\text{A2})$$

where δ is the Dirac delta function and the sum runs over the N particles in the volume considered, one is usually interested in the conditional probability of observing a tracer around one centered at position \vec{x}_o (such as the observer position). In this case, the correlation function can be written

$$C(\vec{x}_o, \vec{x}_o + \vec{r}) = \frac{\delta(\vec{r})}{\rho_0} + \xi(r), \quad (\text{A3})$$

where ξ can be thought of as the “off-diagonal” part of $C(\vec{r})$, and it is physically meaningful only when $r \neq 0$. We can now define the homogeneity scale R_H for a distribution which is locally inhomogeneous but that becomes homogeneous on sufficiently large scales:

$$\left| \frac{3}{R^3} \int_0^R dr \rho(r_i) r^2 - \rho_0 \right| < \rho_0 \quad \forall R \geq R_H, \forall r_i, \quad (\text{A4})$$

where r_i indicates the arbitrary center of a sphere anywhere within the field realization. This definition, written in terms of the correlation function $\xi(r)$, implies:

$$\left| \frac{1}{R^3} \int_0^R dr r^2 \xi(\vec{x}_o + \vec{r}) \right| = 0 \quad \forall R \geq R_H, \forall \vec{x}_o \in \mathcal{V}, \quad (\text{A5})$$

which closely resembles the definition of homogeneity given in Eq. (7), and it is realised for example in the case of pure white noise for which $\xi(r) = 0$.

COMPARISON OF R_V AND R_ρ ACROSS COSMOLOGIES

Whilst the scaling of \mathcal{N} and \mathcal{B}_R becomes approximately proportional asymptotically, the same proportionality does not apply to the numerical values R_v and R_ρ . This is because whilst the numerical value of R_v is determined essentially by the *shape* of $P(k)$ only, R_ρ is also affected by its *amplitude*. This occurs because the crossing of the constant $D_2 = 2.97$ threshold depends largely on the strength and position of the BAO peak in a given cosmology, which can either fall within or above 1% tolerance. Notice that only k modes relatively close to the turnover of the power spectrum impact this numerical value, so varying for example Ω_k has little impact on the value of either $R_{v,\rho}$. To illustrate this more clearly, we plot in Fig. 11 the correlation dimension for a few different cosmologies obtained by varying either one of Ω_m or H_0 keeping the other fixed, or the matter radiation equality $k_{eq} \propto \omega_m h^2$ keeping the present day normalized matter density Ω_m constant.

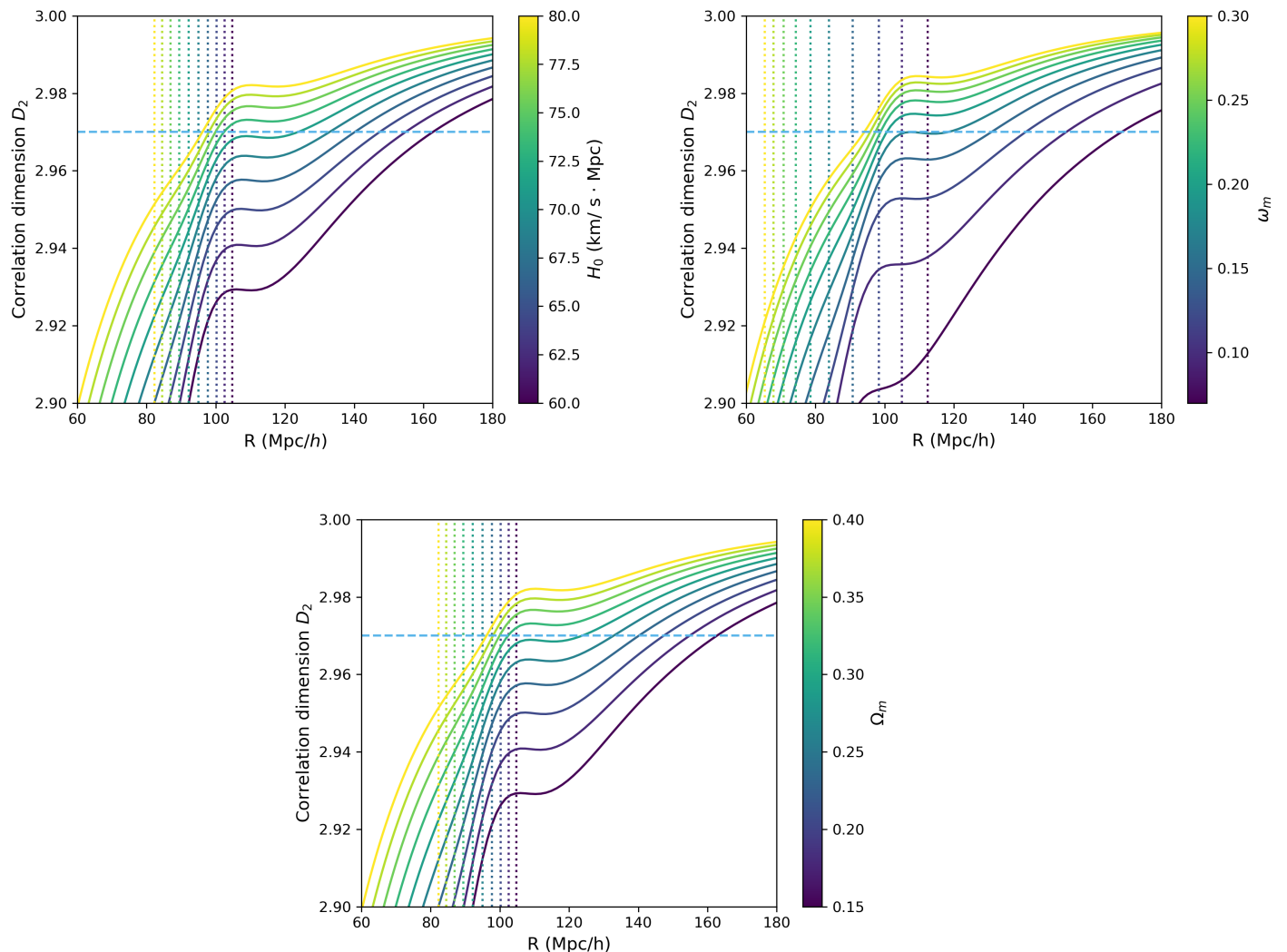


FIG. 11.— The correlation dimension D_2 for a set of fiducial ΛCDM cosmologies varying either Ω_m , H_0 or ω_m (in the latter case keeping constant the normalized present day matter density Ω_m). The blue dashed line shows the $D_2 = 2.97$ threshold defining R_ρ , which, as the plot shows, is intersected by the D_2 curves quite differently depending on the amplitude and position of the BAO peak (despite the fact that all the distributions are statistically homogeneous, sharing the same asymptotic behaviour). On the other hand, the velocity coherence scale R_v (dotted vertical lines) varies more smoothly across cosmologies.

We see that whilst the numerical value of R_v changes smoothly with either of the parameters being varied, the threshold scale R_ρ varies much more abruptly. This is particularly important, since the conversion from redshifts to distances strongly depends on H_0 . For example, a 1.5% variation ΔH_0 around a fiducial value $H_0 = 70 \text{ km/s Mpc}$ can cause shifts in the inferred homogeneity scale of order $\Delta R_\rho \approx 20 \text{ Mpc}/h$.

It is interesting to understand how the R_ρ and R_v statistics behave in truly inhomogeneous spacetimes. As an exercise, we employed the power spectra $P(k)$ computed in a suite of Lemaitre-Tolman-Bondi (LTB) simulations within the BEHOMO⁹ project, first presented in Ref. Marra *et al.* (2022). In particular, we restrict ourselves to a set of simulations in a cubic box of 1 Gpc^3 volume, with a central LTB inhomogeneity of radius $r_b = 400 \text{ Mpc}$ and different values of its average density contrast δ . Fig. 12 shows the snapshots at redshift $z = 0$ of these simulations and the corresponding correlation dimension D_2 , as well as the velocity coherence scale R_v . We notice that the numerical values of both R_v and R_ρ are well below the size of the central inhomogeneity, and therefore one would wrongly conclude that the matter distribution in these boxes is homogeneous. This simple exercise, despite not being rigorous, shows that these estimators should be generally treated as a consistency test, indicating the typical scales of fluctuations in homogeneous cosmologies, rather than direct evidence of homogeneity.

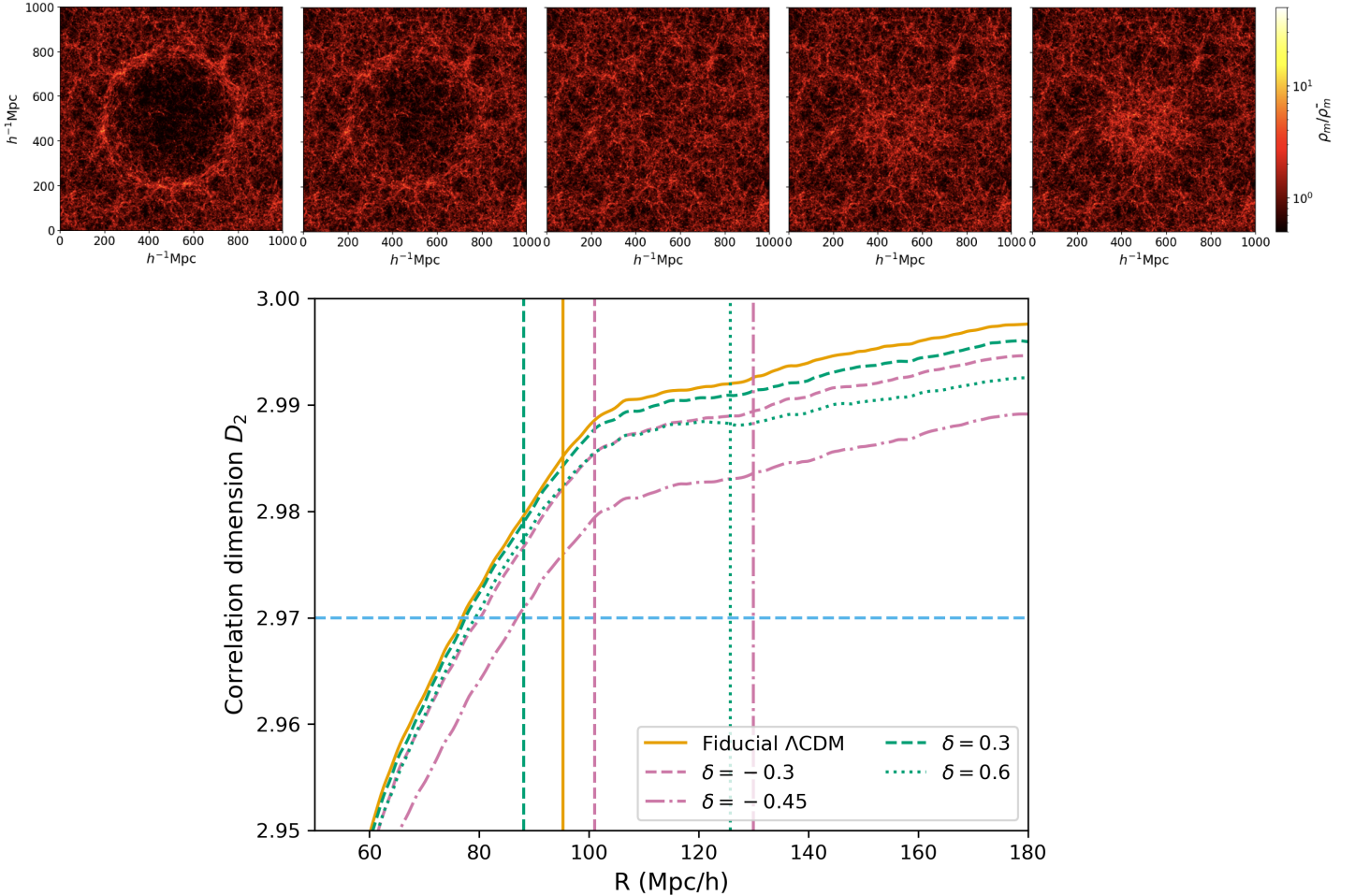


FIG. 12.— *Top*: Snapshots at redshift $z = 0$ of the Λ LTB simulations from the BEHOMO project (Marra *et al.* 2022) considered in this exercise. From left to right, the average density contrasts of the Λ LTB inhomogeneity are $\delta = -0.45, -0.3, 0, 0.3, 0.6$. *Bottom*: The correlation dimension curves and the velocity coherence scales (vertical lines) computed from the above snapshots.

R_V DEPENDENCE ON K_{EQ} AND THE IMPACT OF NON-LINEAR MODES

A theoretical advantage of R_v as a standard ruler is that it is rather simple to understand its cosmological dependence. The zero crossing of $\Psi_{\parallel}(R_v) = 0$ is essentially determined by the shape of the power spectrum, as it is equivalent to the condition

$$\int_0^\infty dk P(k) \left(j_0 - 2 \frac{j_1(kR_v)}{kR_v} \right) = \int_0^\infty dk P(k) \frac{d}{d(kR_v)} [j_1(kR_v)] = 0. \quad (\text{C1})$$

Let us now consider a triangular toy model for the power spectrum $P(k)$ such that

$$P(k) \propto \begin{cases} k & \text{for } k < k_{eq} \\ k^{-3} & \text{for } k > k_{eq} \end{cases}, \quad (\text{C2})$$

⁹ <https://valerio-marra.github.io/BEHOMO-project/>

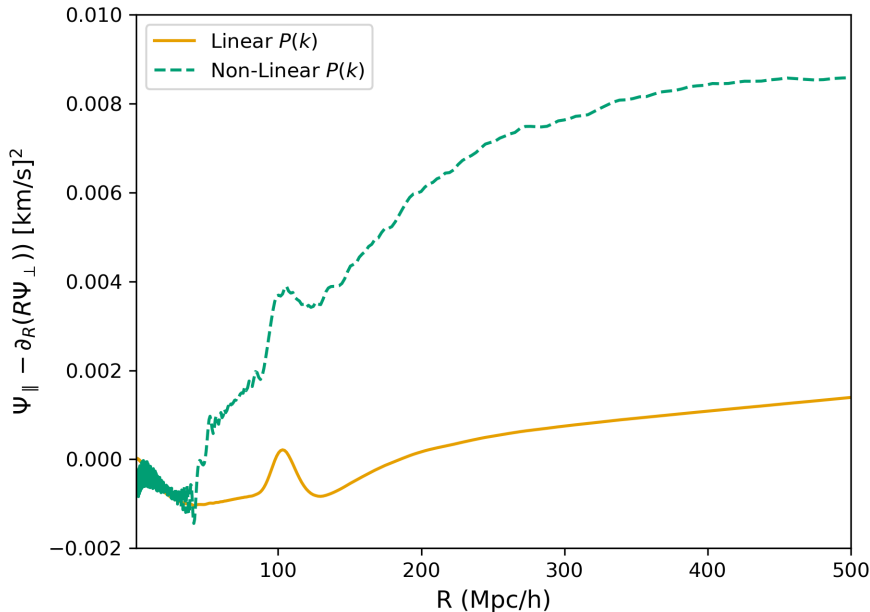


FIG. 13.— The numerical differences between Ψ_{\parallel} and the derivative of $(R\Psi_{\perp})$ computed using fiducial linear (orange) and non-linear (green) power spectra.

in such a way that the integrals can be rewritten as:

$$\int_0^{k_{eq}} dk k \frac{d}{d(kR_v)} [j_1(kR_v)] + \int_{k_{eq}}^{\infty} dk k^{-3} \frac{d}{d(kR_v)} [j_1(kR_v)] = 0. \quad (C3)$$

The integrals above can be solved analytically using integration by parts. A tedious calculation results in the following expression

$$f(R_v) = \frac{1}{R_v^2} \left(1 - \frac{\sin(y)}{y} \right) + \frac{3R_v^2}{30} \left[-\frac{(y^2 + 6) \cos y}{y^4} + \text{Ci}(y) + \frac{(6 + 2y - y^4) \sin y}{y^5} \right] = 0, \quad (C4)$$

where we have defined $y = k_{eq}R_v$. The functional form of the roots of the above equation is highly non-trivial, but one can nevertheless understand that the leading behaviour for $k_{eq} \rightarrow 0$ becomes $R_v \propto 1/k_{eq}$. In the opposite regime, for growing k_{eq} , we can see that R_v behaves as some power law. However, since $k_{eq} \ll 1$, any $n > 0$ polynomial of degree n would be dominated by the linear term. For this reason, we propose the following fitting formula

$$R_v(k_{eq}) \approx \frac{a}{k_{eq}} + bk_{eq} + c, \quad (C5)$$

as in Eq. (26). Fig. 6 shows that this formula is relatively robust even allowing for a non-linear $P(k)$ (which CLASS computes using `halofit`). On the other hand, it is reasonable to ask whether the formula for R_v we obtained from the zero crossing of Ψ_{\parallel} still holds in the presence of non-linear modes, i.e. if Eq. (20) is satisfied.

To show that this is indeed the case, we compute in Fig. 13 the numerical values of Ψ_{\parallel} and the derivative of $R\Psi_{\perp}$ for a fiducial non-linear cosmology. We see that whilst the differences are more pronounced in the non-linear case, they are always small and in particular below 10^{-2} across the distance range probed.

This is expected, since the only physical mechanism that can introduce differences between the two are vorticity effects, which are expected to occur only below ≤ 1 Mpc scales. We conclude that the proposed methodologies to estimate R_v , especially given the precision of current and upcoming cosmological observations, are largely unaffected by any realistic non-linear effect.

REFERENCES

- V. J. Martinez and P. Coles, *ApJ* **437**, 550 (1994).
V. J. Martinez, M.-J. Pons-Borderia, R. A. Moyeed, and M. J. Graham, *Mon. Not. Roy. Astron. Soc.* **298**, 1212 (1998), [arXiv:astro-ph/9804073](https://arxiv.org/abs/astro-ph/9804073).
L. Amendola and E. Palladino, *Astrophys. J. Lett.* **514**, L1 (1999), [arXiv:astro-ph/9901420](https://arxiv.org/abs/astro-ph/9901420).
J. Pan and P. Coles, *Mon. Not. Roy. Astron. Soc.* **318**, L51 (2000), [arXiv:astro-ph/0008240](https://arxiv.org/abs/astro-ph/0008240).
J. Yadav, S. Bharadwaj, B. Pandey, and T. R. Seshadri, *Mon. Not. Roy. Astron. Soc.* **364**, 601 (2005), [arXiv:astro-ph/0504315](https://arxiv.org/abs/astro-ph/0504315).
P. Sarkar, J. Yadav, B. Pandey, and S. Bharadwaj, *mnras* **399**, L128 (2009), [arXiv:0906.3431](https://arxiv.org/abs/0906.3431) [[astro-ph.CO](https://arxiv.org/abs/astro-ph.CO)].
F. Sylos Labini, N. L. Vasilyev, and Y. V. Baryshev, *A&A* **496**, 7 (2009a), [arXiv:0902.0229](https://arxiv.org/abs/0902.0229) [[astro-ph.CO](https://arxiv.org/abs/astro-ph.CO)].
F. Sylos Labini, N. L. Vasilyev, Y. V. Baryshev, and M. López-Corredoira, *A&A* **505**, 981 (2009b), [arXiv:0903.0950](https://arxiv.org/abs/0903.0950) [[astro-ph.CO](https://arxiv.org/abs/astro-ph.CO)].

- F. S. Labini and Y. V. Baryshev, *JCAP* **06**, 021 (2010), arXiv:1006.0801 [astro-ph.CO].
- F. S. Labini, *EPL* **96**, 59001 (2011), arXiv:1110.4041 [astro-ph.CO].
- P. Ntelis *et al.*, *JCAP* **06**, 019 (2017), arXiv:1702.02159 [astro-ph.CO].
- S. Borgani, *Phys. Rept.* **251**, 1 (1995), arXiv:astro-ph/9404054.
- V. J. Martinez and E. Saar, *Proc. SPIE Int. Soc. Opt. Eng.* **4847**, 86 (2002), arXiv:astro-ph/0209208.
- X. Shao, R. Goncalves, C. A. P. Bengaly, G. C. Carvalho, and J. Alcaniz, (2025), arXiv:2507.18720 [astro-ph.CO].
- B. B. Bizarrria, C. P. Novaes, F. Avila, R. Mokeddem, H. H. da Costa, C. A. Wuensche, and G. A. S. Silva, (2025), arXiv:2511.13931 [astro-ph.CO].
- P. Ntelis, A. Ealet, S. Escoffier, J.-C. Hamilton, A. J. Hawken, J.-M. Le Goff, J. Rich, and A. Tilquin, *JCAP* **12**, 014 (2018), arXiv:1810.09362 [astro-ph.CO].
- F. Avila, A. Bernui, R. C. Nunes, E. de Carvalho, and C. P. Novaes, *Mon. Not. Roy. Astron. Soc.* **509**, 2994 (2021), arXiv:2111.08541 [astro-ph.CO].
- M. Scrimgeour *et al.*, *Mon. Not. Roy. Astron. Soc.* **425**, 116 (2012), arXiv:1205.6812 [astro-ph.CO].
- P. K. Aluri *et al.*, *Class. Quant. Grav.* **40**, 094001 (2023), arXiv:2207.05765 [astro-ph.CO].
- R. Watkins *et al.*, *MNRAS* **524**, 1885–1892 (2023).
- A. M. Whitford, C. Howlett, and T. M. Davis, (2023), arXiv:2306.11269 [astro-ph.CO].
- R. Watkins and H. A. Feldman, (2025), arXiv:2512.03168 [astro-ph.CO].
- T. Clifton and N. Hyatt, preprint (2024), arXiv:2404.08586 [astro-ph.CO].
- L. Giani, C. Howlett, K. Said, T. Davis, and S. Vagnozzi, *JCAP* **01**, 071 (2024), arXiv:2311.00215 [astro-ph.CO].
- L. Giani, R. Von Marttens, and R. Camilleri, *Phys. Rev. Lett.* **135**, 071004 (2025a), arXiv:2410.15295 [astro-ph.CO].
- L. Giani, R. Von Marttens, and O. F. Piattella, (2025b), arXiv:2505.08467 [astro-ph.CO].
- Z. G. Lane, A. Seifert, R. Ridden-Harper, and D. L. Wiltshire, *Mon. Not. Roy. Astron. Soc.* **536**, 1752 (2025), arXiv:2311.01438 [astro-ph.CO].
- D. Camarena, K. Greene, J. Houghteling, and F.-Y. Cyr-Racine, *Phys. Rev. D* **112**, 083526 (2025), arXiv:2507.17969 [astro-ph.CO].
- M. Galoppo, L. Giani, M. Hills, and A. Valade, (2025), arXiv:2512.16591 [astro-ph.CO].
- S. Lyall, C. Blake, and R. J. Turner, *Mon. Not. Roy. Astron. Soc.* **532**, 3972 (2024), arXiv:2407.18684 [astro-ph.CO].
- C. Howlett, K. Said, J. R. Lucey, M. Colless, F. Qin, Y. Lai, R. B. Tully, and T. M. Davis, *Mon. Not. Roy. Astron. Soc.* **515**, 953 (2022), arXiv:2201.03112 [astro-ph.CO].
- K. Gorski, *apjl* **332**, L7 (1988).
- E. J. Groth, R. Juszkiewicz, and J. P. Ostriker, *ApJ* **346**, 558 (1989).
- Y. Wang, C. Rooney, H. A. Feldman, and R. Watkins, *MNRAS* **480**, 5332 (2018), arXiv:1808.07543 [astro-ph.CO].
- Y. Wang, S. Peery, H. A. Feldman, and R. Watkins, *ApJ* **918**, 49 (2021), arXiv:2108.08036 [astro-ph.CO].
- R. J. Turner, C. Blake, and R. Ruggeri, *Mon. Not. Roy. Astron. Soc.* **518**, 2436 (2022), arXiv:2207.03707 [astro-ph.CO].
- C. Blake and R. J. Turner, *Mon. Not. Roy. Astron. Soc.* **527**, 501 (2023), arXiv:2308.15735 [astro-ph.CO].
- R. J. Turner, (2024), arXiv:2411.19484 [astro-ph.CO].
- F. Qin, C. Howlett, and L. Staveley-Smith, *Mon. Not. Roy. Astron. Soc.* **487**, 5235 (2019), arXiv:1906.02874 [astro-ph.CO].
- R. J. Turner, C. Blake, and R. Ruggeri, *Mon. Not. Roy. Astron. Soc.* **502**, 2087 (2021), arXiv:2101.09026 [astro-ph.CO].
- A. Gabrielli and F. Sylos Labini, *EPL* **54**, 286 (2001), arXiv:astro-ph/0012097.
- A. Gabrielli, M. Joyce, and F. Sylos Labini, *Phys. Rev. D* **65**, 083523 (2002), arXiv:astro-ph/0110451.
- P. J. E. Peebles, *The large-scale structure of the universe* (1980).
- F. S. Labini and T. Antal, *Astron. Astrophys.* **707**, A254 (2026), arXiv:2511.21585 [astro-ph.CO].
- M. Li, J. Pan, L. Gao, Y. Jing, X. Yang, X. Chi, L. Feng, X. Kang, W. Lin, G. Shan, L. Wang, D. Zhao, and P. Zhang, *ApJ* **761**, 151 (2012), arXiv:1207.5338 [astro-ph.CO].
- P. Andersen, T. M. Davis, and C. Howlett, *Mon. Not. Roy. Astron. Soc.* **463**, 4083 (2016), arXiv:1609.04022 [astro-ph.CO].
- J. Lesgourgues, arXiv e-prints, arXiv:1104.2932 (2011), arXiv:1104.2932 [astro-ph.IM].
- G. B. Poole *et al.*, *MNRAS* **429**, 1902 (2013), arXiv:1211.5605 [astro-ph.CO].
- Y. Lai, C. Howlett, and T. Davis, *JCAP* **10**, 071 (2025), arXiv:2507.11823 [astro-ph.CO].
- N. Aghanim *et al.* (Planck), *Astron. Astrophys.* **641**, A6 (2020), [Erratum: *Astron. Astrophys.* 652, C4 (2021)], arXiv:1807.06209 [astro-ph.CO].
- C. Blake and S. Bridle, *Mon. Not. Roy. Astron. Soc.* **363**, 1329 (2005), arXiv:astro-ph/0411713.
- D. Foreman-Mackey, D. W. Hogg, D. Lang, and J. Goodman, *pasp* **125**, 306 (2013), arXiv:1202.3665 [astro-ph.IM].
- S. Hinton, *Journal of Open Source Software* **1**, 45 (2016).
- C. Saulder *et al.*, (2023), arXiv:2302.13760 [astro-ph.CO].
- K. Said *et al.*, *Mon. Not. Roy. Astron. Soc.* **539**, 3627 (2025), arXiv:2408.13842 [astro-ph.CO].
- e. a. de Jong, *The Messenger* **175**, 3 (2019), arXiv:1903.02464 [astro-ph.IM].
- R. J. Turner *et al.*, (2025), arXiv:2512.03230 [astro-ph.CO].
- V. Marra, T. Castro, D. Camarena, S. Borgani, and A. Ragagnin, *Astron. Astrophys.* **664**, A179 (2022), arXiv:2203.04009 [astro-ph.CO].